

A Soft Wearable Robot for the Shoulder: Design, Characterization, and Preliminary Testing

Ciarán T. O'Neill^{1,2}, Nathan S. Phipps^{1,2}, Leonardo Cappello^{1,2}, *Member, IEEE*, Sabrina Paganoni³,
and Conor J. Walsh^{1,2}, *Member, IEEE*

Abstract— In this paper, we present a soft wearable robot for the shoulder which has the potential to assist individuals suffering from a range of neuromuscular conditions affecting the shoulder to perform activities of daily living. This wearable robot combines two types of soft textile pneumatic actuators which were custom developed for this particular application to support the upper arm through shoulder abduction and horizontal flexion/extension. The advantage of a textile-based approach is that the robot can be lightweight, low-profile, comfortable and non-restrictive to the wearer, and easy to don like an item of clothing. The actuator's ability to fold flat when not in use allows the robot to be almost invisible under clothing, potentially allowing the user to avoid any stigma associated with using assistive devices in public. To abduct the arm, a textile-based pneumatic actuator was developed to fit within the axilla to push the arm upwards, while a pair of smaller actuators pivot the abduction actuator to allow for horizontal extension and flexion. The individual textile actuators were experimentally evaluated before being integrated into a wearable garment. Human subject testing was performed to evaluate the ability of the robot to assist the arm by monitoring changes in biological muscle activity when comparing the robot powered on and off. Preliminary results show large reductions in muscular effort in targeted muscles, demonstrating the feasibility and promise of such a soft wearable robot for the shoulder.

I. INTRODUCTION

Several neuromuscular conditions like stroke, spinal cord injury, muscular dystrophy and ALS, result in a limited ability to perform activities of daily living (ADLs), which ultimately leads to a loss of independence. The ability to move the upper limb and to interact with the environment is critical in sustaining a person's ability to perform ADLs. A limited ability to perform ADLs is associated with both an increased risk of mortality [1] and up to a 10 year reduction in life expectancy [2]. To this extent, the shoulder joint is particularly important because it is the first joint of the upper limb kinematic chain and its impairment drastically limits the function of the whole limb.

It is possible to find a number of existing solutions in the literature that aim to support the arm after a loss of shoulder function. Some [3]–[6] are intended as robotic rehabilitation devices capable of fine motion control and large force application. These devices enable good control over position

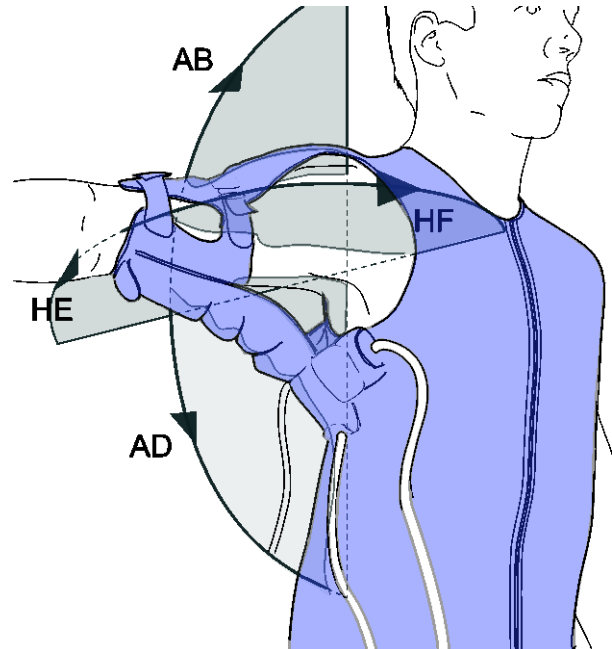


Figure 1: The Soft Wearable Robot for the Shoulder with anatomical motions. Abduction (AB), Adduction (AD), Horizontal Flexion (HF) and Horizontal Extension (HE).

and force for performing rehabilitation protocols but were not intended to be easily portable or used outside of a clinical setting. Several lightweight systems [7]–[11] have been developed to address the size and mass requirements for a portable assistive device, which is particularly useful in cases where it is impossible to restore normal function through rehabilitation therapy. To date, the majority of these systems operate by having cables pull the arm upwards with reaction loads borne by the torso. The inherent advantages of these cable driven systems are that they are lightweight at distal locations as they allow for remotely located actuation systems. Often, they require some form of structure protruding from the shoulder or upper limb to generate a sufficient lever arm to reduce the cable force required to achieve a given joint torque.

Soft robotics is a quickly growing field which makes use of highly compliant materials to create inherently soft actuators and sensors that lead to creative designs as demonstrated from the work of the community [12]. Previous work in pneumatic-powered soft wearable robots has leveraged McKibben style actuators to assist with ankle plantar flexion [13], knee extension/flexion [14] and wrist rehabilitation [15] while others have employed bending actuators to assist with hand function [16], [17] and rotary actuators to assist with elbow

¹ The Wyss Institute for Biologically Inspired Engineering, Harvard University, Cambridge, MA, 02138 and

² John A. Paulson School of Engineering and Applied Sciences, Harvard University, Cambridge, MA, 02138

³ Department of Physical Medicine and Rehabilitation, Harvard Medical School, Spaulding Rehabilitation Hospital, Boston, Massachusetts, 02129 (Corresponding author email: walsh@seas.harvard.edu)

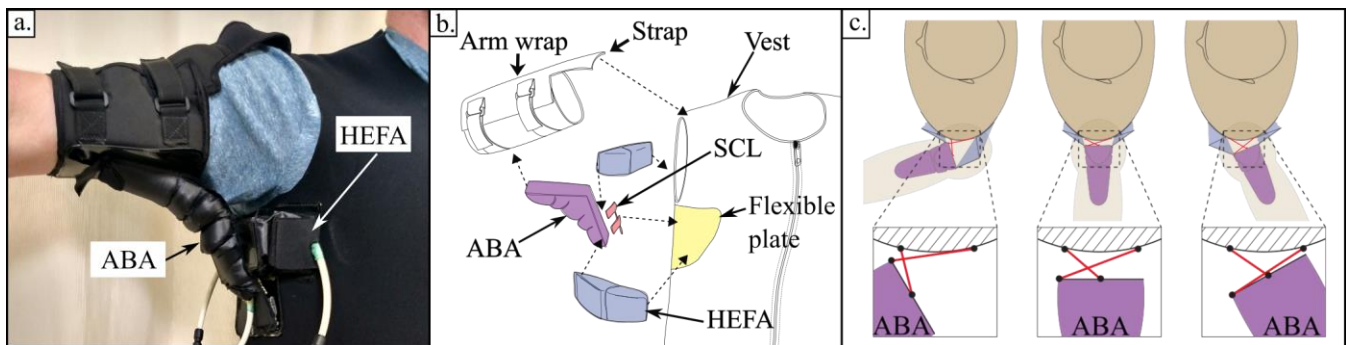


Figure 2: The effect of inflation pressure on the shoulder using the Abduction actuators (ABA) with the Horizontal Extension/Flexion Actuator (HEFA) also visible, b) Exploded view of the final robot including the Soft Cruciate Linkage (SCL), c) Overhead view of the SCL working to achieve HF and HE. Red lines indicate the asymmetric SCL linkages.

extension/flexion [18]. The advantage of these soft actuators is that they are inherently compliant and do not over-constrain the user as the frame where the forces are applied is the user's own skeletal structure: thus improving comfort and safety. The removal of the requirement to accurately match the kinematics of the device with the human simplifies the donning of soft wearable robots and virtually eliminates the need to adjust the device thereafter. The lack of rigid members limits the occurrence of peak contact forces as the soft actuators more readily deform to distribute applied forces. Textile based soft actuators can be very lightweight and can collapse down and fold flat when not pressurized resulting in a mechanically transparent system. Additionally, textile based soft actuators leverage existing manufacturing methods already employed by the apparel industry which may lower the barrier to mass production and enable low cost systems.

Our research aims to demonstrate that an assistive robot for shoulder manipulation based on textile soft pneumatic actuators has the potential to deliver sufficient assistive forces to reduce muscular activity in impaired individuals while maintaining a low profile and weight.

In this paper, we present a soft wearable robot for the shoulder to assist shoulder abduction/adduction and shoulder horizontal flexion/extension (Figure 1). Section II offers a detailed description of the two different textile based pneumatic actuators that comprise the wearable robot, as well as an experimental characterization of these actuators. The robot was evaluated through human subject experiments to assess its performance and the results are presented in Section III.

II. SOFT WEARABLE ROBOT FOR THE SHOULDER

A. Design Considerations

To enable a discrete wearable robot, a goal was set to minimize the profile of the actuators, ideally repositioning them to the underside of the arm. This is important to increase acceptability by the user and by the community in daily life. A key factor in minimizing the robot's profile was to minimize the volume of the actuators while still delivering the requisite output forces and moments. A further consequence of reducing the profile of the actuators is that the available moment arms were also reduced. The total moment/force that can be generated by a given size of a pneumatic actuator is a function of the supply pressure which we chose to restrict to 200kPa (29PSI) as this is the pressure limit of many small electric

compressors. This resulted in a tradeoff being made between actuator sizing and the desired output moment/force. To abduct the arm, moments on the order of 15-20Nm (calculated using anthropomorphic data [19]) need to be generated to overcome the weight of the arm and up to 1kg additional load held by the user.

B. Wearable Robot Overview

The final wearable robot consists of a vest to which two types of textile-based actuators are attached (Figure 2a, b). The vest is constructed of neoprene (Seattle Fabrics, USA) and reinforced with a flexible plate below the axilla to securely anchor the Soft Cruciate Linkage (SCL) and the Horizontal Extension/Flexion actuators (HEFAs). The Abduction actuator (ABA) is coupled to the upper arm via a padded arm wrap which has Velcro to allow for adjustment to individual users. To prevent the wrap from sliding, the wrap is tethered to the vest via a strap (Figure 2b). The HEFAs are sewn to the edges of the ABA and to the flexible plate on the vest, while the SCL is used to connect the ABA to the flexible plate on the vest.

C. Soft Cruciate Linkage (SCL)

A four-bar linkage system, mimicking the cruciate ligaments, was developed to connect the ABA to the vest as illustrated (in red) in Figure 2b, c. The linkage allows the rotation of the ABA about the vertical axis while minimizing horizontal and vertical displacement. An asymmetric arrangement of the four-bar linkage was chosen to allow for maximum HF while limiting HE which is depicted in the lower portion of Figure 2c. Kevlar reinforced sail cloth (Dimension, USA) was used to make these linkages. The four-bar linkage mechanism is further explained in section II E.

D. Abduction Actuator (ABA)

The ABA actuator previously mentioned is comprised of a segmented chamber made of inextensible textile (Weathermax, USA) attached to a spine consisting of two flexible plates connected via a flexible hinge (Figure 3a). The flexible plates help resist misalignment between segments and are located between two layers of textile with the dividing stitching between them acting as a hinge. An oversized bladder made of heat-sealed TPU (Fiberglast, USA) is inserted into the textile component to form an inflatable airtight volume. The bladder is oversized as its function is solely to retain air, while the fabric structure is designed to absorb and distribute the stresses due to pressurization. Shoulder adduction i.e. the motion assisted by gravity, is not actuated as the robot is

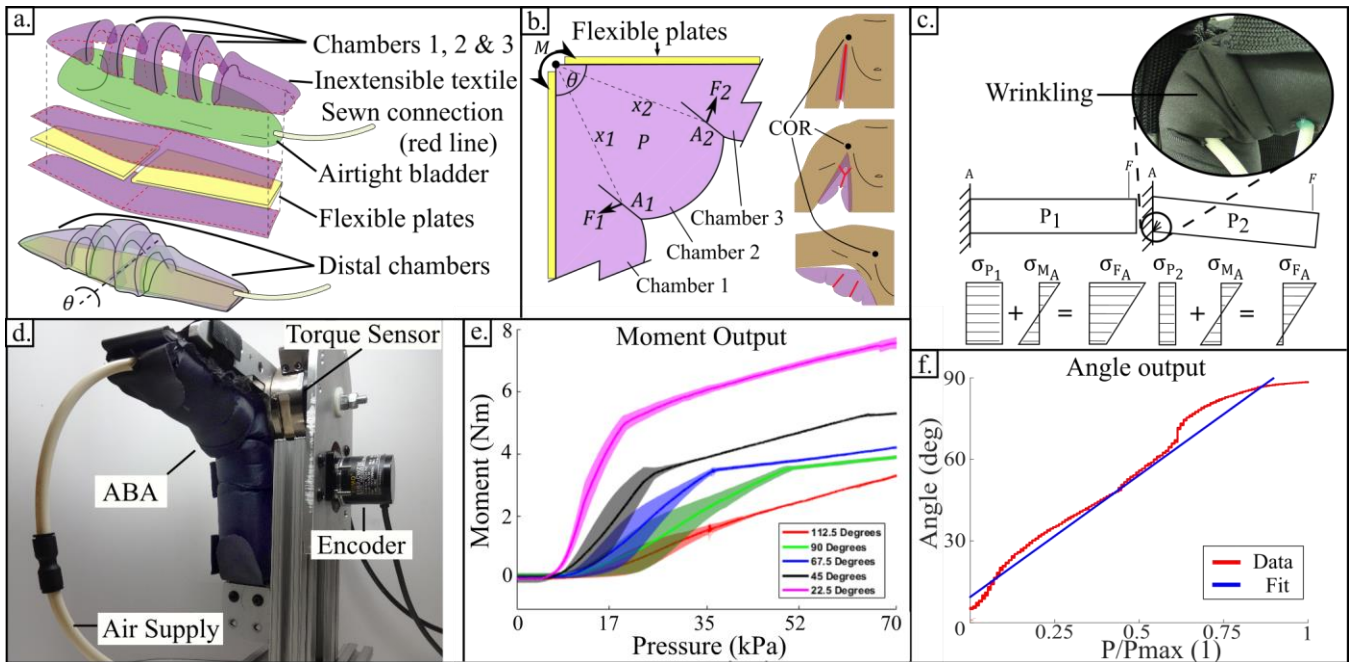


Figure 3: a) Exploded view of the ABA, b) Force diagram of the ABA and visualization of contact area highlighted in red with center of rotation (COR) of the shoulder. $x_{1,2}$ is the distance from the COR to the center of pressure of $A_{1,2}$, which is used to calculate $F_{1,2}$ using the internal pressure P , c) Effect of wrinkling with identical moments applied where $P_1 > P_2$. P_2 provides insufficient tensile preload to prevent buckling. d) ABA test fixture, e) Experimental results of moment output at fixed angles where shaded area represents standard deviation, f) Experimental results of relationship between pressure and angle under fixed load where P_{max} is the maximum pressure recorded.

initially intended to target upright (i.e. non-reclined) users. Shoulder adduction is achieved by simply deflating the ABA in a controlled fashion.

The main chamber of the actuator has been segmented into five sub-chambers to limit the effects of wrinkling. Wrinkling results in a dramatic reduction in the actuator's stiffness and ability to support load. Wrinkling occurs when the local stress in the textile becomes compressive as textiles buckle under compressive stress. This phenomena has been investigated and experimentally validated in studies exploring the nucleation criteria of wrinkles in inflatable beams [20] and inflatable cones [21]. Inflation of the actuator generates a tensile stress preload in the textile to overcome any compressive stresses present and this effect is illustrated in Figure 3c where the greater pressure P_1 ($P_1 > P_2$) generates sufficient tensile stress (σ_{P1}) throughout the beam to exceed the compressive stress from the applied moment (σ_{MA}), thus preventing the formation of a wrinkle ($\sigma_{FA} > 0$). Should one segment wrinkle, it does not cause the entire actuator to buckle as would be the case with a single segment actuator. By reducing the wrinkling pressure, i.e. the minimum pressure to avoid wrinkling, it is reasonable to assume that a more precise relationship between pressure and output moment for a given angle can be achieved.

The total moment generated by the actuator is approximately the sum of the moments between chambers 1, 2 & 3 in Figure 3a, b. The two distal chambers (Figure 3a) minimally contribute to moment generation given their reduced moment arm. The theoretical center of rotation (COR) of the actuator is located at the joint of the two flexible plates rather than co-located with the shoulder joint. In a rigidly framed system, a prismatic joint would be required to

allow for translation of the arm wrap during rotation. However, due to the flexibility of the plates and the compliance of the textiles elements, the actuator may be directly coupled with the human body without over-constraining the user.

To evaluate and characterize the abduction actuator, a test fixture was developed (Figure 3d). It comprises a 6-axis load cell (Gamma 15-50, ATI-IA, USA) to record the applied moments and a 1024 count quadrature encoder (E6B2, Sparkfun, USA) to record actuation angle. Pressure was monitored with a 700kPa pressure transducer (100PAAA5, Honeywell, USA). All data was captured at 500Hz using a NI PCIe 6259 DAQ (National Instruments, USA) and Simulink (Mathworks, USA). The angle of actuation could be fixed or left free to rotate. Static moment tests were performed by locking the actuator at a number of discrete angles to evaluate the moment output of the actuator with respect to pressure. Additionally, we sought to verify the linearity of the segmented actuator output motion with respect to pressure by allowing for free rotation and applying a fixed load as the actuator was inflated.

Figure 3e and Figure 3f report the results of our experimental evaluation of the ABA. In Figure 3e, the relationship between pressure and output moment at a number of fixed angles is presented. Two distinct regions exist, the first of which is a region with greater variability as indicated by the increase in SD that we attribute to the changing contact area between the chambers due to the wrinkles followed by a linear region where we assume wrinkling does not occur due to the increased internal pressure and the contact area remaining relatively constant. The changing contact area is due to the folds of a wrinkle containing some textile which is

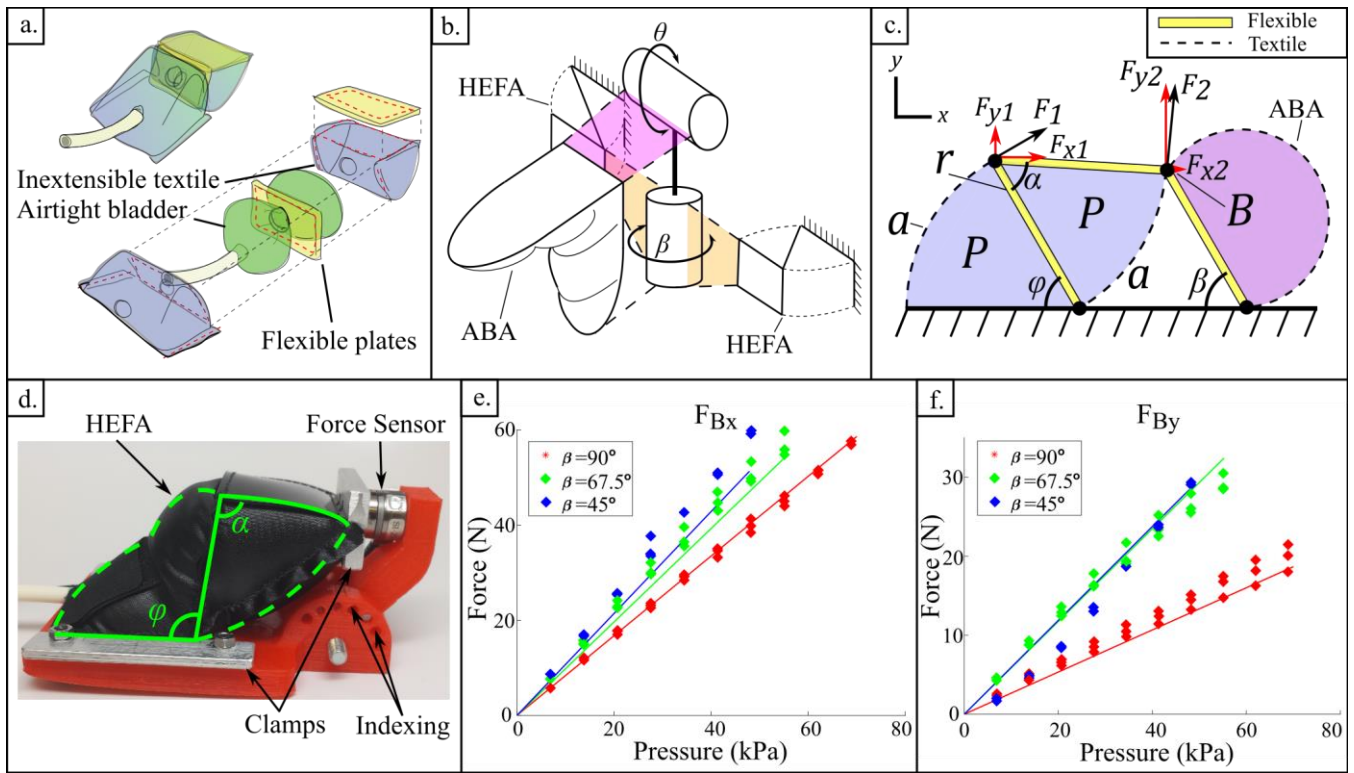


Figure 4: a) Exploded diagram of the HEFA, b) Kinematic model of ABA and HEFA c) Overhead force diagram of HEFA attached to an ABA where ground is to the torso, d) HEFA test fixture, e) Comparison for experimental force in x and numerical model where the model is represented by the solid lines and the experimental data by the asterisks., f) Comparison for experimental force in y and numerical model.

then no longer part of the contact area as it's within the fold. In Figure 3e it is also evident that the generated moment decreases as the angle θ increases. This is an expected behavior as for smaller values of θ , there is additional contact area between the sub-chambers of the actuator, increasing the effective area for moment generation and the moment arm with a resulting increase in applied moment (red lines illustrated in Figure 3b). The area for moment generation continues to decrease with increasing actuator angle θ as each segment tends towards a quasi-spherical equilibrium state. In Figure 3f, a linear relationship ($R^2 = .98$) is apparent between input pressure and the output angle θ under fixed load. This linear relationship between pressure and abduction angle is ideal as it greatly simplifies the open loop control of the actuator.

E. Horizontal Extension/Flexion Actuator (HEFA)

To actuate the second DoF of the shoulder, i.e. horizontal extension/flexion motion, we developed a Horizontal Extensor/Flexor actuator (HEFA) (Figure 4a). To decouple abduction motion from horizontal extension/flexion, we designed the HEFA to apply rotational motion to the ABA (Figure 4b). To achieve both extension and flexion, an antagonistic pair of actuators is required as gravity cannot be employed as is the case with adduction.

Each HEFA consists of two wedge-shaped chambers in series with a common air supply, which when combined with the SCLs, results in a 4-bar linkage that transmits compressive force to the ABA when the HEFA is inflated, as represented in Figure 4c. As with the ABA, the HEFA is constructed of an inextensible textile with an internal airtight TPU bladder. The

trajectory of the interface point between the HEFA and the ABA (point B, Figure 4c) is the arc traced by the edge of the ABA as it rotates about its opposite edge. When uninflated, the HEFA folds flat with α and ϕ equal to 0 degrees. By varying the length of the flexible plates, their width w and the arc a (Figure 4c), it is possible to achieve different stroke and force profiles. The top flexible plate generates a moment from the inflation of the top chamber while also transmitting force from the moment generated by the bottom chamber. No flexible plate is required under the bottom chamber as the bottom chamber is mounted to the flexible plate of the vest. We observed that the angle α is consistently smaller than the angle ϕ at any pressure and we theorize that this effect is due to the larger deformation of the top flexible plate with respect to the bottom plate.

The following equations describe the forces generated by the single chambers of the actuator; as derived from the free body diagram depicted in Figure 4c:

$$F_{x1} = \frac{Prw \sin\phi}{2} \quad (1)$$

$$F_{x2} = \frac{k(i)Prw \sin(\phi - \alpha)}{2}, \quad (2)$$

$$F_{y2} = \frac{k(i)Prw \cos(\phi - \alpha)}{2}. \quad (3)$$

F_2 decreases as α approaches $\alpha_{\text{equilibrium}}$. $\alpha_{\text{equilibrium}}$ is the maximum α angle that is achievable by the pressurized top chamber and it is calculated based on the arc length a of the textile and r . Once $\alpha_{\text{equilibrium}}$ is reached, the pressure applied to the flexible plates is balanced by the stress in the textile, reducing F_2 to 0. This effect is captured by the empirically

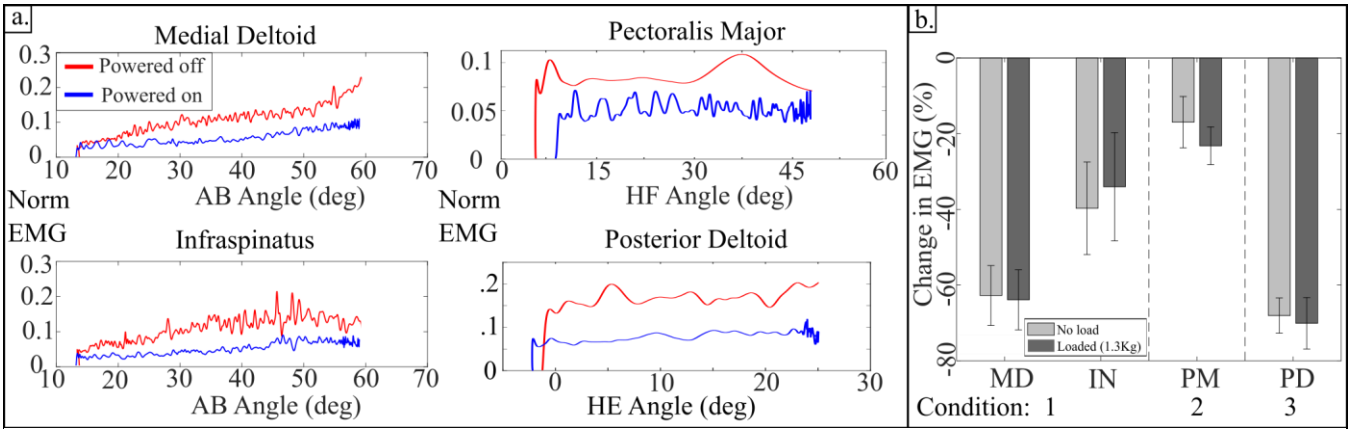


Figure 5: a) Sample processed EMG data taken from all unloaded trials of a subject under each condition. Final angles were determined as the minimum angle achieved by the robot across trials. For this subject, the device was only capable of abducting the arm to 59°, horizontally flex to 48° and extend to 26° due to device slippage and migration under load. b) EMG changes between robot powered on and powered off in targeted muscles for each condition.

determined function k that describes the proximity to equilibrium state:

$$k(i) \approx (1 - e^{-3(i-1)}), \quad (4)$$

where:

$$i = \frac{\alpha}{\alpha_{equilibrium}}. \quad (5)$$

The total forces along x and y directions at point B that the HEFA transmits to the ABA are the sum of the two contributions:

$$F_{Bx} = F_{x1} + F_{x2}, \quad (6)$$

$$F_{Bx} = \frac{Prw(\sin(\varphi) + k(i)\sin(\varphi - \alpha))}{2}, \quad (7)$$

$$F_{By} = F_{y2}. \quad (8)$$

To experimentally evaluate the performance of the HEFA, a test fixture (Figure 4d) was developed to measure the force output at a number of discrete angles. A miniature 6-axis load cell (Nano17, ATI-IA, USA) was used to measure the applied forces. Pressure was monitored with a 700kPa pressure transducer (100PAAA5, Honeywell, USA) and all data was acquired at 500Hz by a NI PCIe 6259 DAQ (National Instruments, USA) and processed in Simulink (Mathworks, USA).

The magnitude of the estimated forces correlates well with the recorded experimental data as observable in Figure 4e and Figure 4f. The forces in the x -direction have an average R^2 value of 0.94 while the forces in the y -direction have an average R^2 value of 0.71.

III. HUMAN SUBJECT TESTING

A study was conducted on three healthy male subjects (mean±sd: 26±3.6 years, 80.6±4.0 kg, 1.79±0.055 m) to examine the ability of the robot to assist the arm in abduction, horizontal extension and horizontal flexion in reducing the wearers biological muscle effort. Subjects were asked to perform a number of arm motions with the robot worn and in a powered on and powered off state. Four double differential surface electromyography (sEMG) sensors (Trigno Wireless EMG, Delsys, USA) were placed on top of the Medial Deltoid (MD), Posterior Deltoid (PD), Pectoralis Major (PM) and

Infraspinatus (IN) muscles of the subject to record muscle activity during the tests [22], [23]. These muscles were selected due to their use during ADLs [24]. Other minor muscles assist with the performance of ADLs; however, they were not monitored for this first proof of concept human trial. Arm and shoulder movement was recorded using a motion capture system (VICON, UK) with 24 reflective markers. EMG signals were recorded at 2160Hz and motion capture data was recorded at 120Hz. The study was approved by the Harvard Medical School Institutional Review Board. Four conditions were tested; during condition 1 the subjects were instructed to abduct their arm to approximately 90 degrees. During conditions 2 and 3 the subjects were instructed to horizontally flex and extend their arm respectively while maintaining 90 degrees of abduction. A fourth condition was carried out where the subject was instructed to perform isometric maximum voluntary contractions (MVC) in abduction, horizontal extension and horizontal flexion while their arm was held securely at the starting position of each condition. This last condition provided maximum muscle effort values for normalization of EMG data. Each condition consisted of four modalities, i.e. robot powered off, robot powered on, no load, loaded (1.3kg) and each modality was repeated for three trials. Periodic auditory cues were given to the subject during each trial to ensure consistent velocities between robot powered off and robot powered on modalities to remove any contraction velocity artifacts from the EMG recording [25]. No discomfort or muscle fatigue of the shoulder and upper body was reported by any participant throughout the study. In condition 1, the targeted muscles were the MD and IN, in condition 2 the PM and in condition 3 the PD.

During post-processing, the raw EMG signals were full wave rectified and filtered with a 4th order Butterworth low pass filter with a corner frequency of 10Hz. The filtered EMG signals were then normalized with respect to the MVC [22]. EMG data acquired from the execution of condition 1, 2 and 3 of a single subject, averaged between all three trials, is depicted in Figure 5a, where the comparison between the robot state (powered on/off) with no load is noticeable. The robot is capable of achieving the minimum ROM required to perform 83% of ADLs [24] (Robot ROM: 55.1°±5.3° AB, 56.7°±9.7° HF, 28.3°±3.5° HE). Figure 5b shows the average reduction of EMG signal when the robot is powered on for each

TABLE 1: STUDY CONDITIONS AND OUTCOMES

Condition	Target Muscle	Modality	Average Reduction	Max	Condition	Target Muscle	Modality	Average Reduction	Max
1	MD	Robot off, no load	62.75	90.49± 1.73%	2	PM	Robot off, no load	16.94	40.15± 3.48%
		Robot on, no load	±7.90%				Robot on, no load	±6.77%	
		Robot off, load	63.89				Robot off, loaded	23.20	
		Robot on, load	±7.92%				Robot on, loaded	±4.98%	
1	IN	Robot off, no load	39.72	69.80± 3.42%	3	PD	Robot off, no load	68.05	80.87± 4.80%
		Robot on, no load	±12.23%				Robot on, no load	±4.64%	
		Robot off, loaded	34.03				Robot off, loaded	70.09	
		Robot on, loaded	±14.31%				Robot on, loaded	±6.80%	

representative muscle under experimental conditions 1, 2 and 3 executed both without and with load. The results are additionally broken down in TABLE 1 above. The average reductions in Figure 5b are calculated as the decrease in the average EMG signal over equivalent ranges of motion between robot on and off over for all trials in each individual modality and condition. Maximum reductions are included from unloaded modalities in each condition. Importantly, no increases in muscle activity in untargeted muscles in any trial were observed which indicates that the robot does not unintentionally load any of the other major muscles of the shoulder. As a component of the deltoid, the PD contributes both to abduction and horizontal extension motions. To isolate the effect of the assistance provided by the HEFA we compared PD activation between condition 2, where the PD is not involved in horizontal flexion motion, and condition 3, where the PD contributes to horizontal extension motion. Average reductions of $65.27 \pm 2.48\%$ and $56.71 \pm 3.61\%$ respectively were seen in PD activity during condition 1 which corresponds to a reduction of $2.78 \pm 8.23\%$ and $13.38 \pm 3.61\%$ for the horizontal extension motion

IV. CONCLUSION AND FUTURE WORK

A preliminary design and evaluation of a soft wearable robot for the shoulder that includes compact and lightweight textile pneumatic actuators is presented. The prototype described here comprises three individual actuators: one for abduction of the shoulder and two for bidirectional control of horizontal flexion and extension. The total worn component weighs 0.48 kg, folds flat and does not limit user's motion when unpowered. The actuators were individually tested and characterized on a test bench. Experiments on healthy human subjects were conducted to validate the design and results support the use of the proposed wearable robot to assist a variety of patient populations with the execution of ADLs. These results pave the way for the use of soft wearable robots to promote independence in scenarios where cost, portability, ease of maintenance and reduced form factor are paramount, such as home and community use. The techniques employed to fabricate the proposed wearable robot are highly scalable to mass production by the apparel industry.

Future work on this device will investigate optimal textile patterning, SCL sizing and flexible plate geometry [26] to

increase the range of motion of the robot in addition to improving moment generation over the desired range of motion. The design of the vest must also be modified for use by either sex as currently there is no accommodation for a bust. Anchoring to the wearer is critically important to device operation as slippage results in reduced forces and range of motion. Anchoring may be improved in future iterations through the use of inextensible textile components and non-slip materials. The integration of soft sensors to measure the angles between various components will provide valuable information for control. For this prototype, pressure was supplied by an offboard compressor but a portable system with integrated control and power electronics is under development towards a fully mobile solution.

Future biomechanical analysis will monitor additional EMG sensors on other muscles in the shoulder and torso to better characterize the effects of the device on the user and determine if unintentional loading of is occurring in previously untargeted muscles.

ACKNOWLEDGMENT

The authors would like to thank Jonathan Foster and Dr. Fausto Panizzolo for their assistance with the collection of EMG and motion capture data, Lauren Bizarro with the IRB protocol and Tracy Jiang for assistance manufacturing the actuators and the device. This work was supported by the National Science Foundation (Grant #s 1454472 and 1317744), the Wyss Institute for Biologically Inspired Engineering and the Harvard John A. Paulson School of Engineering and Applied Sciences.

REFERENCES

- [1] L.-W. Wu *et al.*, "All-cause mortality risk in elderly individuals with disabilities: a retrospective observational study," *BMJ Open*, vol. 6, no. 9, p. e011164, 2016.
- [2] I. M. Majer, W. J. Nusselder, J. P. Mackenbach, B. Klijs, and P. H. M. Van Baal, "Mortality risk associated with disability: A population-based record linkage study," *Am. J. Public Health*, vol. 101, no. 12, pp. 9–15, 2011.
- [3] Y. Mao and S. K. Agrawal, "Design of a cable-driven arm exoskeleton (CAREX) for neural rehabilitation," *IEEE Trans. Robot.*, vol. 28, no. 4, pp. 922–931, 2012.
- [4] M. Simkins, H. Kim, G. Abrams, N. Byl, and J. Rosen, "Robotic unilateral and bilateral upper-limb movement training for stroke survivors afflicted by chronic hemiparesis," *IEEE Int. Conf. Rehabil. Robot.*, pp. 1–6, 2013.

- [5] B. Kim and A. D. Deshpande, "Controls for the shoulder mechanism of an upper-body exoskeleton for promoting scapulohumeral rhythm," *IEEE Int. Conf. Rehabil. Robot.*, vol. 2015–Septe, pp. 538–542, 2015.
- [6] K. D. Fitle, A. U. Pehlivan, and M. K. O'Malley, "A robotic exoskeleton for rehabilitation and assessment of the upper limb following incomplete spinal cord injury," *2015 IEEE Int. Conf. Robot. Autom.*, pp. 4960–4966, 2015.
- [7] I. Galiana, F. L. Hammond, R. D. Howe, and M. B. Popovic, "Wearable Soft Robotic Device for Post-Stroke Shoulder Rehabilitation : Identifying Misalignments," 2012.
- [8] D. Park, I. Koo, and K. J. Cho, "Evaluation of an improved soft meal assistive exoskeleton with an adjustable weight-bearing system for people with disability," *IEEE Int. Conf. Rehabil. Robot.*, vol. 2015–Septe, pp. 79–84, 2015.
- [9] T. G. Sugar *et al.*, "Design and control of RUPERT: A device for robotic upper extremity repetitive therapy," *IEEE Trans. Neural Syst. Rehabil. Eng.*, vol. 15, no. 1, pp. 336–346, 2007.
- [10] M. Xiloyannis, L. Cappello, K. D. Binh, C. W. Antuvan, and L. Masia, "Preliminary design and control of a soft exosuit for assisting elbow movements and hand grasping in activities of daily living," *J. Rehabil. Assist. Technol. Eng.*, vol. 4, pp. 1–15, 2017.
- [11] I. Gaponov, D. Popov, S. J. Lee, and J. Ryu, "Auxilio : A Portable Cable-driven Exosuit for Upper Extremity Assistance," *Int. J. Control. Autom. Syst.*, vol. 15, no. 1, pp. 73–84, 2016.
- [12] D. P. Holland, E. J. Park, P. Polygerinos, G. J. Bennett, and C. J. Walsh, "The Soft Robotics Toolkit : Shared Resources for Research and Design," vol. 1, no. 3, pp. 224–230, 2014.
- [13] M. Wehner *et al.*, "A lightweight soft exosuit for gait assistance," *Proc. - IEEE Int. Conf. Robot. Autom.*, pp. 3362–3369, 2013.
- [14] Y. L. Park, J. Santos, K. G. Galloway, E. C. Goldfield, and R. J. Wood, "A soft wearable robotic device for active knee motions using flat pneumatic artificial muscles," *Proc. - IEEE Int. Conf. Robot. Autom.*, pp. 4805–4810, 2014.
- [15] G. Andrikopoulos, G. Nikolakopoulos, and S. Manesis, "Motion control of a novel robotic wrist exoskeleton via pneumatic muscle actuators," *IEEE Int. Conf. Emerg. Technol. Fact. Autom. ETFA*, vol. 2015–October, 2015.
- [16] P. Polygerinos, K. C. Galloway, S. Sanan, M. Herman, and C. J. Walsh, "EMG controlled soft robotic glove for assistance during activities of daily living," *IEEE Int. Conf. Rehabil. Robot.*, vol. 2015–September, pp. 55–60, 2015.
- [17] P. Polygerinos, Z. Wang, K. C. Galloway, R. J. Wood, and C. J. Walsh, "Soft robotic glove for combined assistance and at-home rehabilitation," *Rob. Auton. Syst.*, vol. 73, pp. 135–143, 2015.
- [18] A. Wilkening, H. Stoppler, and O. Ivlev, "Adaptive assistive control of a soft elbow trainer with self-Alignment using pneumatic bending joint," *IEEE Int. Conf. Rehabil. Robot.*, vol. 2015–September, pp. 729–734, 2015.
- [19] P. de Leva, "Adjustments to Zatsiorsky-Seluyanov's segment inertia parameters," *J. Biomech.*, vol. 29, no. 9, pp. 1223–1230, 1996.
- [20] S. L. Veldman, "Wrinkling prediction of cylindrical and conical inflated cantilever beams under torsion and bending," *Thin-Walled Struct.*, vol. 44, no. 2, pp. 211–215, 2006.
- [21] W. Changguo, D. U. Zhenyong, and T. A. N. Huifeng, "A Novel Method for Wrinkling Analysis of Membrane Inflated Cone in Bending," *Acta Mech. Sin.*, vol. 26, no. 4, pp. 617–623, 2010.
- [22] H. J. Hermens, B. Freriks, C. Disselhorst-Klug, and G. Rau, "Development of recommendations for SEMG sensors and sensor placement procedures," *J. Electromyogr. Kinesiol.*, vol. 10, no. 5, pp. 361–374, 2000.
- [23] E. F. Delagi, A. Perotto, J. Iazzetti, and D. Morrison, *Anatomical Guide For The Electromyographer : The Limbs And Trunk, fourth edition by Aldo O. Perotto*. Springfield IL, 2005.
- [24] D. J. Magermans, E. K. J. Chadwick, H. E. J. Veeger, and F. C. T. Van Der Helm, "Requirements for upper extremity motions during activities of daily living," *Clin. Biomech.*, vol. 20, no. 6, pp. 591–599, 2005.
- [25] T. Masuda *et al.*, "Influence of contraction force and speed on muscle fiber conduction velocity during dynamic voluntary exercise," *J. Electromyogr. Kinesiol.*, vol. 11, no. 2, pp. 85–94, 2001.
- [26] D. Kim and R. B. Gillespie, "Origami Structured Compliant Actuator (OSCA)," *IEEE Int. Conf. Rehabil. Robot.*, pp. 259–264, 2015.